RESILIENT INFRASTRUCTURE
June 1–4, 2016

EFFECT OF WIND SPEED AND TERRAIN EXPOSURE ON THE WIND PRESSURES FOR ELEVATED STEEL CONICAL TANKS

Ahmed Musa
Ph.D Candidate, Western University, Canada

Haitham Aboshosha
Research Engineer, Boundary Layer Wind Tunnel Laboratory, Western University, Canada

Ashraf El Damatty
Professor and chair, Western University, Canada

ABSTRACT

Steel liquid storage tanks in the form of truncated cones are commonly used as containment vessels for water supply or storing chemicals. A number of failures have been recorded in the past few decades for steel liquid tanks and silos under wind loading. A steel conical tank vessel will have a relatively small thickness making it susceptible to buckling under wind loads especially when they are not fully-filled. In this study, a wind tunnel pressure test is performed on an elevated conical tank in order to estimate the external wind pressures when immersed into a boundary layer. The tested tank configuration represents combined conical tanks where the cone is capped with a cylinder. In addition, the effect of terrain exposure and wind speed on the pressure values and wind forces is assessed. The mean and rms pressure coefficients are presented for different test cases in addition to the mean and rms total drag forces that are obtained by integrating the pressure coefficient over the tank model's surface. It is found that the total mean and rms drag forces are highly-dependent on Reynolds number which is a function of wind speed and they have a maximum value at mid-height for the lower cylinder, at top for the conical part, and at bottom for the upper cylindrical part.

Keywords: conical steel tanks, wind pressure, wind tunnel pressure test, Reynolds number, terrain exposure

1. INTRODUCTION

Steel conical-shaped liquid storage tanks are widely used for fluid storage. An elevated steel conical tank consists of a steel vessel made of welded steel panels connected to a steel base which is in turn resting on a concrete slab. Depending on the required pressure head, a conical tank is elevated through a hollow cylindrical concrete shaft. Steel vessels are advantageous to be used as they are composed of prefabricated steel panels simplifying the erection procedure and reducing the construction costs. A conical tank is referred as a combined one when the truncated cone is capped with a cylindrical part as shown in Figure 1.

Figure 1: Combined conical tank (http://www.caldwellwatertanks.com)

Being constructed of steel, a conical tank vessel will have a relatively small thickness making it susceptible to buckling under wind loads especially when they are not fully-filled. A number of failures in the form of tank vessel buckling has been noticed in the past (Flores and Godoy 1998, Godoy 2007, and Rossana and Godoy 2010) for cylinderical tanks and silos. Therefore, many studies were performed in order to estimate the wind pressures acting on circular cylindrical tanks. The flow over a circular cylinder have been extensively studied and three flow regimes have been identified depending on the flow Reynolds number, Re. These flow regimes are sub-critical flow, critical flow, and super-critical flow.

In the subcritical, Re ranges from 300 to $1.5x10^5$-$2.0x10^5$ and the corresponding mean drag coefficient C_{dm} is about 1.2. By increasing Re up to around $4.0x10^5$, the flow enters the critical or transitional regime where C_{dm} sharply decrease to around 0.2 which is known as drag-crisis. Finally, the supercritical regime takes place once Re exceeds $4.0x10^6$ where C_{dm} increases again. The three flow regimes with their characteristic C_{dm} values and Re ranges are based on a two-dimensional cylinder model in a smooth flow. This might be applicable for a slender cylindrical model where the aspect ratio has no effect on the flow characteristics. The surface roughness was also found to affect the characteristics of the flow regimes. A rougher surface causes the critical Reynolds number range to be lower than that for a smooth cylinder with the minimum drag coefficient is higher for the rougher surfaces (ESDU 1980). The effect of the cylinder aspect ratio on the flow regimes was studied experimentally (Fox and West 1993, Baban and So 1991, and Okamoto and Sunabahiri 1992) and it was generally agreed that C_{dm} of a finite-length cylinder are smaller than those of a 2D cylinder.

Sabransky and Melbourne (1987) performed wind tunnel pressure tests for a grain storage silo with circular cylindrical walls and conical roof. In their tests, they considered different roof pitches and height-to-diameter ratios. They found that drag coefficients increase with height for the cylinder due to the incident velocity profile and the three dimensional flow over the free end of the cylinder. Macdonald et al. (1988) carried out wind tunnel pressure tests for low-rise cylindrical structures at Reynolds number Re exceeding 2 X $l0^5$. Reynolds number represents the ratio between convective to viscous wind forces and is defined as vd/ν, where v is the mean velocity, d is a characteristic dimension and ν is the viscosity. Wall and roof pressures were recorded for tanks with different aspect ratios and Re. It was found that increasing the aspect ratio increases the magnitude of the maximum mean suction on the wall. On the roof, it was found that near the leading edge and conical apex, high suction takes place. Another finding was that wall pressures become independent of Re when Re is greater than 1 X 10^5.

Falcinelli et al. (2011) performed Computational Fluid Dynamics CFD simulations for a cylindrical tank with a conical roof to evaluate the wind pressures acting on the tank. They considered the effect of having an upstream hill on the tanks' measured pressures. The results showed that tank location with respect to a hill has a significant influence on the pressures with maximum recorded pressures when the tank is located at the top of a hill. Uematsu et al. (2014) and Uematsu et al. (2015) investigated wind force coefficients for designing open-topped oil storage tanks experimentally using wind tunnel tests and analytically using finite element buckling analysis for the case of isolated tank and group of two to four tanks. The studies revealed that positive wind pressure is the main parameter affecting the buckling capacity of the tanks.

Most of the studies found in the literature are related to estimating wind pressures for cylindrical tanks and silos. However, it is expected that wind pressures for the case of conical tanks would be different than cylindrical tanks due to wall inclination and therefore more studies on conical tanks are needed. Few studies are available in the literature related to wind actions on conical tanks. Parammasivam and Tamura (2007) performed pressure wind tunnel test for an elevated conical tank model at a Reynolds number of 10^5. It was found that the pressure distribution in the circumferential direction matches the distribution over a cylindrical tank. However, the pressure values increase with the height above the ground reaching their maximum at the top of the cone. This was related to the effect of separated flow, recirculating flow, and the tip effects. Sundaravadivel et al. (2009) compared the results of the latter wind tunnel testing with those obtained from CFD employing Reynolds-averaged Navier–Stokes (RANS) equations. The predicted patterns of pressure coefficients were found to be in reasonably good agreement with the wind tunnel testing for the elevated conical tank except for the wake zone, which cannot be handled by RANS. The main conclusion was that flow over the cone section is a three-dimensional compared to the shaft section which can be considered as a two-dimensional one.

The above mentioned studies related to conical tanks provided good insights on understanding the flow characteristics around conical tanks. However, they did not address the effect of upstream terrain nor the tank geometric parameters

on the external wind pressures in addition to the effect of varying the approaching wind speed. Studying such parameters and how they influence external wind pressures is the main scope of the current study where a wind tunnel pressure test is conducted on a scaled elevated combined conical tank model. The outputs of the pressure test in terms of mean and rms pressures and drag forces are presented and discussed.

2. EXPERIMENTAL SETUP

The pressure tests are conducted at the Boundary Layer Wind Tunnel Laboratory (BLWTL) at Western University, Canada. The tunnel has a length of 39 m, width of 3.4 m, and a height of 2.5 m as shown in Fig 2a. Proper turbulence intensity and incoming velocity profile are adjusted using floor roughness elements, end barrier, and spires as shown in Figures 2b to 2d. Wind velocity is varied during the test between 4.6 m/s and 18.3m/s leading to a range of Re between $9.2x10^4$ and $3.66x10^5$ at top height.

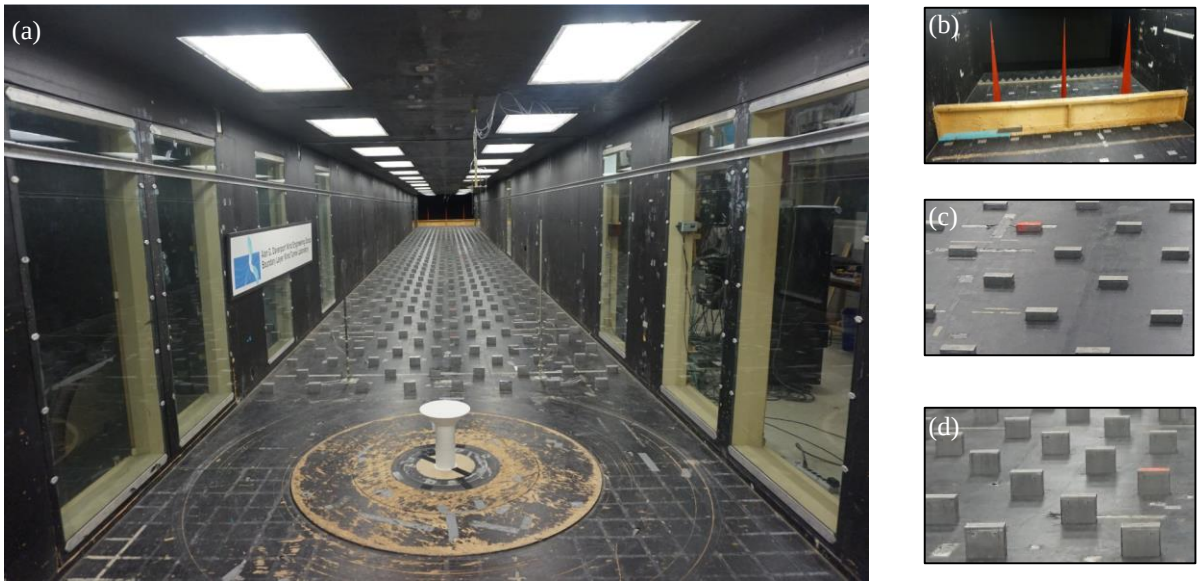

Figure 2: (a) Boundary layer wind tunnel (BLWTL), Western university, Canada; (b) Installed spires and barrier; (c) Roughness blocks for open terrain; (d) Roughness blocks for suburban terrain

Two terrain exposures are considered in this study: open flat terrain (Exposure C: z_0=0.03 m) and suburban terrain (Exposure B, z_0=0.25 m), where z_o is the aerodynamic roughness. This aerodynamic roughness z_o increases with the increase of the ground roughness and higher value of z_o leads to a steeper velocity profile as shown in Figure 3. The figure also shows the exposures measured at the wind tunnel compared with the target profiles defined in the ASCE (2012). The figure shows a good agreement between the measured profiles and the targeted profile regarding mean wind speed and turbulence intensity.

A set of 8 test cases is considered in this study including two terrain exposures (i.e., open and suburban) and four wind speeds. Different wind speed values are considered in order to study the effect of varying Reynolds number on the external wind pressure values. The chosen wind speed values are 4.6, 9.1, 13.7, and 18.3 m/s at a height of 147 cm above the tunnel floor level. For each test case, a duration of 128 sec with a sampling frequency of 400 Hz is recorded. The wind speed is measured and monitored through a set of installed pitot tubes in the wind ward side.

3. MODEL PROPERTIES

The considered combined conical tank has a height of 40m, a wall angle of 45° and a top diameter of 30m. A length scale of 1:100 is considered in the test as shown in Figure 4a. The conical tank model is constructed using fused deposition modeling (FDM) and consists of four parts as shown in Figure 4: (a) Supporting cylindrical shaft referred as LC, (b) Conical tank vessel referred as CP, (c) Upper cylindrical vessel referred as UC, and (d) Tank roof. Pressure

taps are distributed around the circumference of the tank model as shown in Figure 4c at different heights to estimate the height-wise variation of the wind pressures. Each level of pressure taps is given an index representing the part of the model where it is located and the percentage ratio of the level's height to the total height of this part as shown in Figure 4b. Regarding the circumferential distribution of the pressure taps, they are denser along the sides of the model with respect to the wind direction where the flow separation is expected to occur in order to accurately capture the pressure distribution.

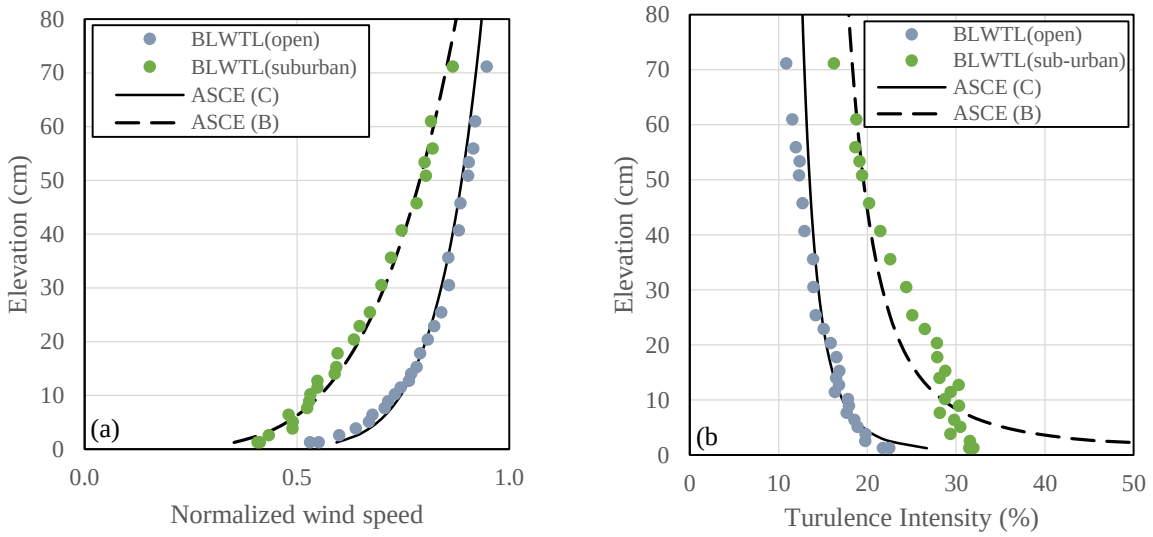

Figure 3: (a) Mean wind speed profiles; (b) Turbulence intensity for open and suburban terrain exposures

Typically, pressure taps on the model are connected through pneumatic tubing to electronic pressure scanners, each capable of handling 16 different taps. The data acquisition system records the digitized signals from the scanning modules at a scanning sampling rate of 400Hz. The reference dynamic pressure in the free stream above the boundary layer is recorded similarly. All of this data is stored for the determination of maximum, minimum, mean and rms pressure values for each tap. More details on the experimental technique for pressure models can be found in BLWTL (2007)

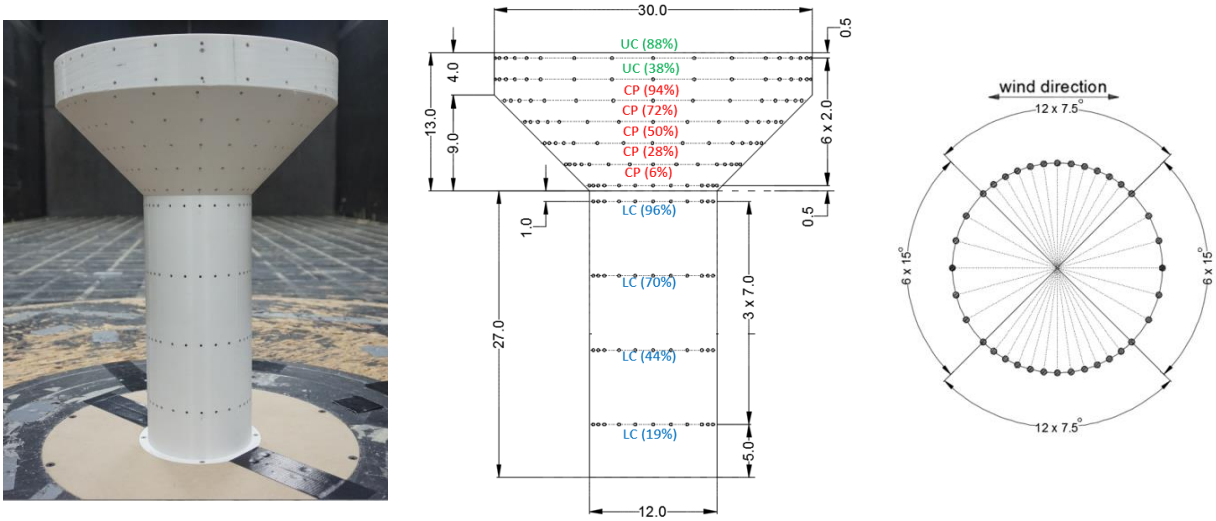

(a) (b) (c)

Figure 4: (a) Combined tank model, (b) Pressure taps' layout (Dimensions are in cm), (c) Circumferential distribution of pressure taps

4. TEST RESULTS

As mentioned, pressure time histories are recorded simultaneously at each pressure tap. These records are analyzed in order to obtain mean and rms pressures in addition to total drag and lift forces acting on various components of the conical tank model. The mean and rms pressures are reported in terms of mean and rms pressure coefficients C_{pm} and C_{prms} defined as:

[1] $$C_{pm} = \sum_1^n C_p(t)/n$$

[2] $$C_{prms} = \sqrt{\sum_1^n \left(C_p(t) - C_{pm} \right)^2 / n}$$

where $(C_p(t) = p(t) - p_o / 0.5\,\rho\,\bar{V}^2)$ with p(t) is the pressure measured at time instance t, p_o is the mean static reference pressure, ρ is the air density, n is the number of recorded time increments, and $\bar{V}$ is the wind speed at 40 cm height which represents the roof height of the combined model.

4.1 Mean pressures

Distribution of the mean pressure coefficient C_{pm} over the tank walls is investigated for different test cases. Effect of changing wind speeds and terrain exposure on C_{pm} variation with the circumferential angle θ is discussed. A circumferential angle θ=0° represents the windward side (i.e. stagnation point), while θ=180° represents the leeward side angle. Figure 5 shows the effect of changing wind speed on C_{pm} values where the horizontal axis represents the circumferential angle θ and the vertical axis represents the C_{pm} values. Each subplot shows C_{pm}-θ relation for the three model components at different levels corresponding to certain wind speed.

A typical C_{pm} variation with the angle θ can be divided into four zones as shown in Figure 5d: zone 1 represents the positive pressure region starting from the stagnation point to the point of zero pressure, zone 2 extends from the end of zone 1 till the point of lowest pressure (maximum negative pressure), zone 3 extends from the end of zone 2 till the point where the pressure becomes constant, and zone 4 represents the nearly constant negative pressure region acting on the leeward cylinder region.

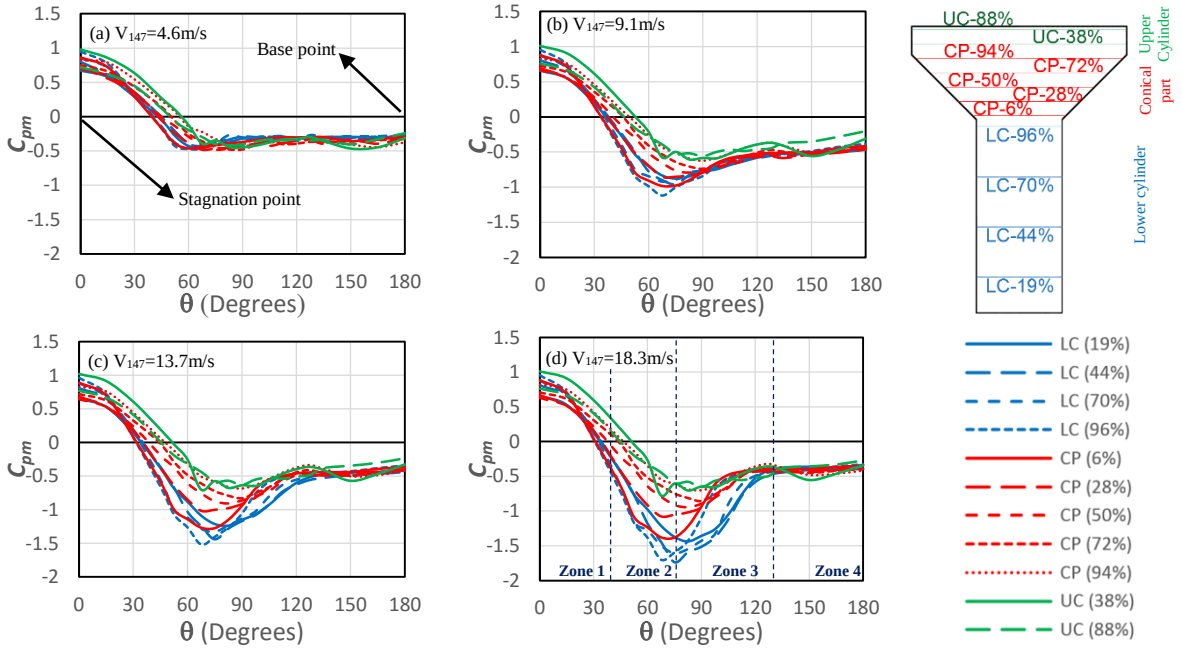

Figure 5: Distribution of C_{pm} at different levels for open exposure test cases: a) V_{147}=4.6m/s , b) V_{147}=9.1m/s, c) V_{147}=13.7m/s, and d) V_{147}=18.3m/s

By investigating Figure 5 regarding the effect of wind speed on C_{pm} variation, it is found that: the angle at which zone 2 starts shifts away from the stagnation point at higher levels and the maximum negative C_{pm} value increases at higher wind speeds; the base C_{pm} is reduced for higher wind speeds except for the case of the lower wind speed (V_{147cm}= 4.6m/s). Under such a low speed the flow is in the sub-critical regime which may be the reason for that. On the other hand, Figure 6 shows the effect of changing the terrain exposure on C_{pm} values. Each subplot shows C_{pm}-θ relation for the three model components at different levels corresponding to the two considered terrain exposures, i.e., open and suburban, at two wind speeds. By investigating Figure 6 regarding the effect of the terrain exposure on C_{pm} variation for different model parts, it is found that: suburban exposure results in slightly lower positive and slightly higher negative C_{pm} values due to the lower wind speeds compared to the open terrain exposure; the difference in C_{pm} values is reduced for higher levels as the wind speed profiles corresponding to the two exposures approach each other as we go far from the ground.

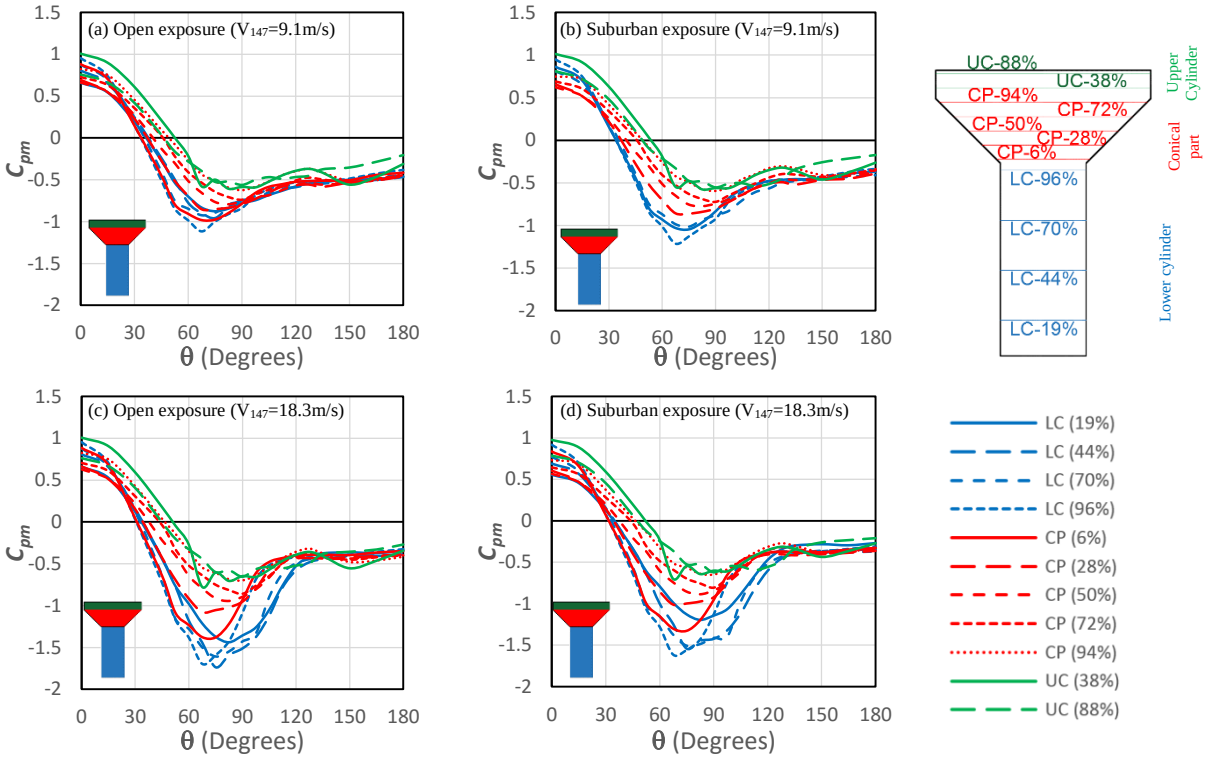

Figure 6: Distribution of C_{pm} at different levels for test case: (a) Open exposure (V_{147}=9.1m/s), b) Suburban exposure (V_{147}=9.1m/s), c) Open exposure (V_{147}=18.3m/s), and d) Suburban exposure (V_{147}=18.3m/s)

4.2 Fluctuating Pressure

In this subsection, fluctuating pressures are examined and the variation of the rms pressure coefficient C_{prms} over the tank walls is investigated for different test cases. The effect of changing wind speed and terrain exposure on C_{prms} variation with the circumferential angle θ is discussed.

Figure 7 shows the effect of changing the wind speed on C_{prms} values where the horizontal axis represents the circumferential angle θ and the vertical axis represents the C_{prms} values. Each subplot shows C_{prms}-θ relation for the three model components at different levels corresponding to certain wind speed. By investigating Figure 7 regarding the effect of the wind speed on C_{prms} variation, it is found that: C_{prms} distribution have a more clear peak plateau near zones 2 and 3 for higher wind speeds for both lower cylinder and conical part; C_{prms} values are higher in zones 2, 3 and lower in zones 1,4 for higher wind speeds for both lower cylinder and conical part; C_{prms} values over the upper cylinder are reduced in zones 2, 3 and 4, with the exception of the lower wind speed (v_{147}=4.6m/s) in zone 4, for higher wind speeds.

Figure 8 shows the effect of changing terrain exposure on C_{prms} values. Each subplot shows C_{prms}-θ relation for the three model components at different levels corresponding to the two considered terrain exposures, i.e., open and suburban, at two wind speeds. By investigating Figure 8 regarding the effect of the terrain exposure on C_{prms} variation, it is found that: C_{prms} lower cylinder values are smaller for the suburban exposure compared to the open terrain exposure; C_{prms} values for the conical part are higher for the suburban exposure in zones 1 and 2 and lower in zones 3 and 4 compared to the open terrain exposure except for the lower wind speed (v_{147}=4.6m/s) where C_{prms} values is lower for the suburban exposure in all zones; C_{prms} for the upper cylinder has lower values in zones 1, 2 and 3 and higher values in zone 4 for the suburban exposure compared to the open terrain exposure except for the lower wind speed (v_{147}=4.6m/s) where C_{prms} values is lower for the suburban exposure in all zones.

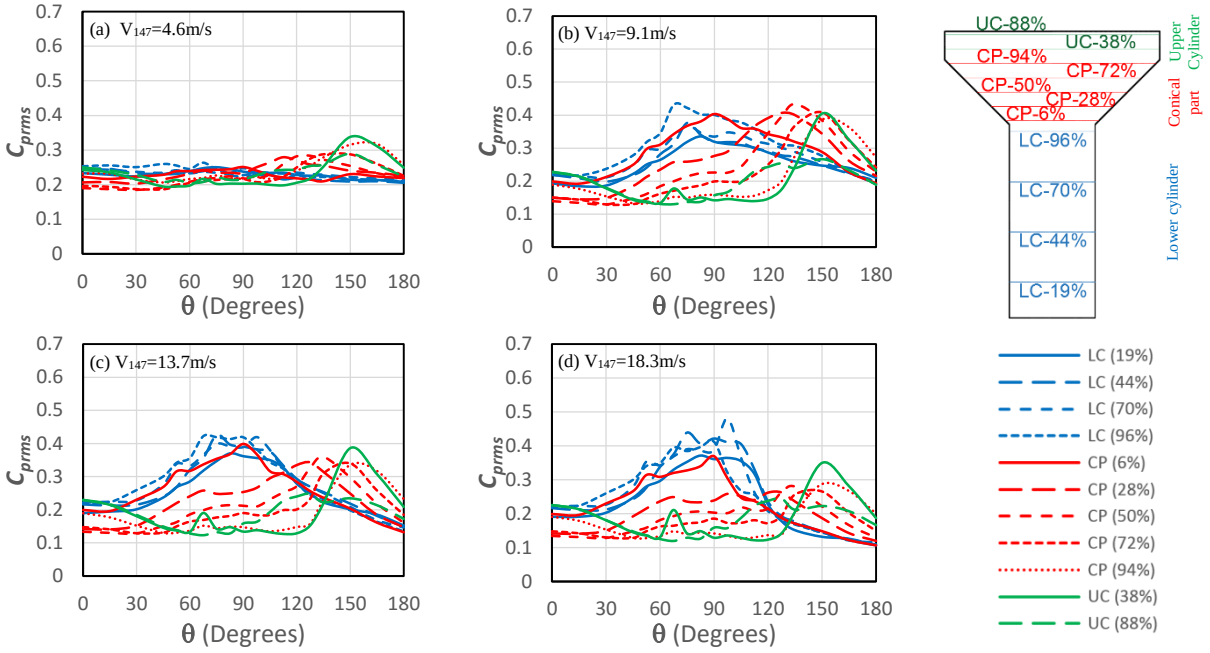

Figure 7: Distribution of C_{prms} at different levels for open exposure test cases: a) V_{147}=4.6m/s , b) V_{147}=9.1m/s, c) V_{147}=13.7m/s, and d) V_{147}=18.3m/s

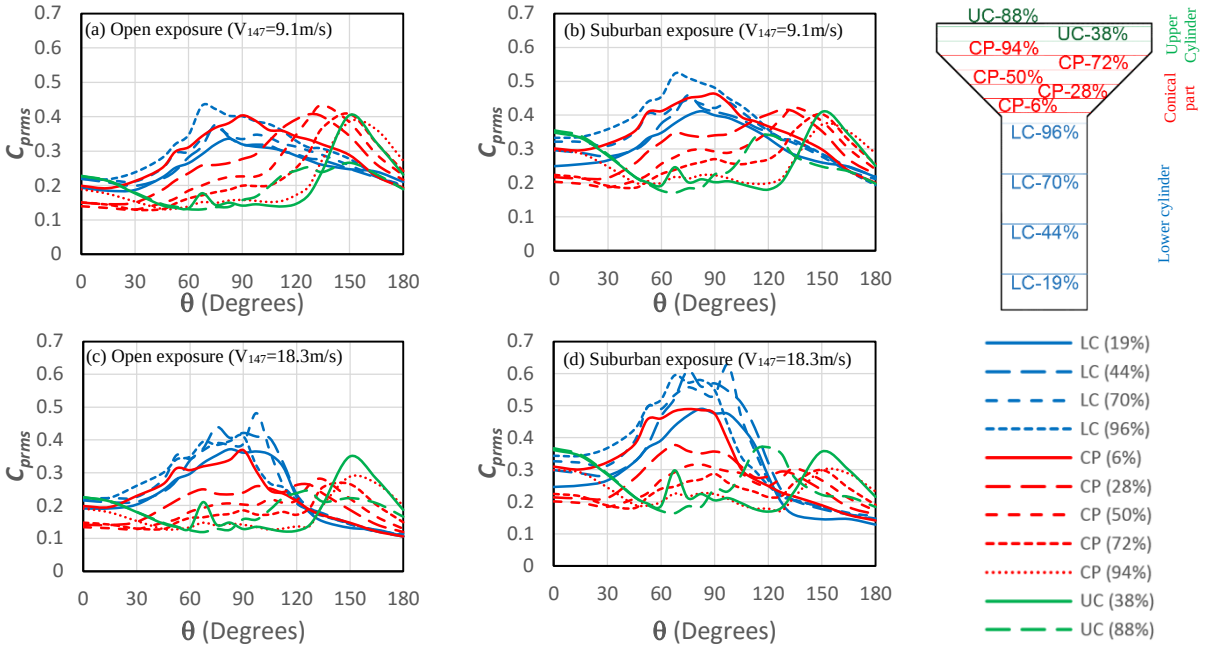

Figure 8: Distribution of C_{prms} at different levels for test case: (a) Open exposure (V_{147}=9.1m/s), b) Suburban exposure (V_{147}=9.1m/s), c) Open exposure (V_{147}=18.3m/s), and d) Suburban exposure (V_{147}=18.3m/s)

4.3 Mean Drag Forces

Drag force, F_D, acting on the tank is evaluated and reported in terms of the drag coefficient, C_d. The relationship between force F_D and coefficient C_d is given by.

[3] $$C_d = F_D / 0.5\,\rho V^2 A$$

where ρ is the air density, V is the reference wind speed and A is the projected area subjected to wind pressure. The coefficient C_d is evaluated by integrating the pressure coefficient C_p acting at various taps using the following expression, where A_i is the tributary area around each tap.

[4] $$C_d = \sum_{i=1}^{N} C_{pi} \cos\theta_i \, A_i \, / A$$

Mean drag coefficient, C_{dm}, can be evaluated from the C_d time series at each pressure taps' level. Figure 9a shows the distribution of C_{dm} along the tank height for the eight tested cases corresponding to four wind speeds (i.e. V_{147} = 4.6, 9.1, 13.7, and 18.3 m/s) within the two considered terrain exposures (i.e. open and suburban). The following findings can be obtained from this figure: (1) C_{dm} distribution for the lower cylinder has a maximum value around the mid-height except for the lowest wind speed (i.e., v_{147}=4.6m/s) where the max C_{dm} is at the top height, (2) For the conical part, C_{dm} is increasing linearly with the height excluding the lowest wind speed (i.e., v_{147}=4.6m/s), (3) For the top cylinder, C_{dm} is reduced with the height, (4) C_{dm} values for the suburban exposure are lower compared to the open terrain for all parts.

As discussed earlier, the mean drag force for circular structures is dependent on Reynolds number Re which represents the ratio of inertial to viscous forces within the flow. As a result, the variation of the mean overall drag coefficient C_{dovm} with Reynolds number for different model parts is investigated. The mean overall drag coefficient C_{dovm} is obtained for each part by integrating the C_{dm} values shown in Figure 9a over the height of this part. Figure 9b shows the variation of C_{dovm} with Re for different parts. As the wind speed varies with height and the model diameter is not constant for the conical part, the considered Re is based on the wind speed and tank diameter at the top of each part. It is found that the mean overall coefficient is dependent on the Re and the following findings can be deduced from Figure 9b: (1) For the lower cylinder, C_{dovm} is reduced with increasing Re expect for the case of open terrain with

lowest wind speed (i.e., v_{147}=4.6m/s), (2) For the conical part, C_{dovm} is reduced with increasing Re expect for the case of open terrain with lowest wind speed (i.e., v_{147}=4.6m/s), (3)For the upper cylinder, C_{dovm} is slightly reduced with increasing Re, (4) C_{dovm} is found to be higher for all parts tested within the open terrain due to the higher wind speed profile compared to the suburban one.

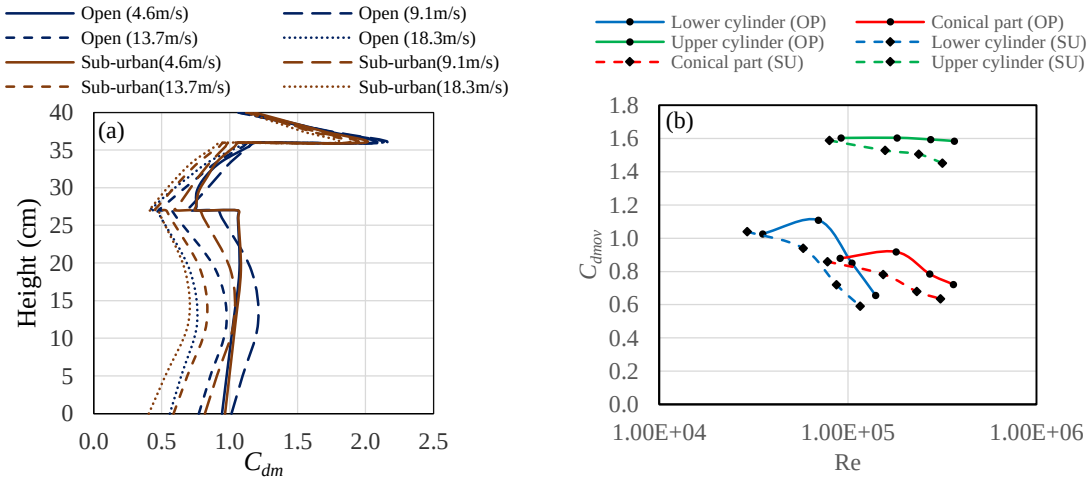

Figure 9: (a) Height-wise distribution of mean drag coefficient C_{dm}, (b) Variation of mean overall drag coefficient C_{dovm} for each part with Re

4.4 Fluctuating Drag Forces

In addition to the mean value, rms drag C_{drms} coefficient is also evaluated from the drag time series. Figure 10a shows the distribution of C_{drms} along the tank height for the eight considered test cases corresponding to four wind speeds (i.e. V_{147} = 4.6, 9.1, 13.7, and 18.3 m/s) within the two considered terrain exposures (i.e. open and suburban). The following findings can be obtained with regards to the rms drag coefficient C_{drms}: (1) C_{drms} distribution for the lower cylinder has a maximum value around the mid-height, (2) For the conical part, C_{drms} increases with the height, (3) For the top cylinder, C_{drms} reduces with the height, (4) C_{drms} values for the suburban exposure are higher compared to the open exposure due to higher turbulence intensity.

Similar to the case of mean overall drag, the variation of the rms overall drag C_{dovrms} with Reynolds number for different model parts is investigated. The rms overall drag C_{dovrms} coefficient is obtained for each part by integrating the C_{drms} values shown in Figs. 10a over the height of this part. Figure 10b shows the variation of C_{dovrms} with Re for different parts where the considered Re is based on the wind speed and tank diameter at the top of each part. The following findings can be obtained from Figure 10b for the rms overall drag coefficient C_{dovrms}: (1) For the lower cylinder, C_{dovrms} is reduced with increasing Re for different testing levels expect for the test case within open terrain with lowest wind speed (i.e., v_{147}=4.6 m/s), (2) For the conical part, C_{dovrms} is reduced with increasing Re for the cases expect for the case within open terrain with lowest wind speed, (3) For the upper cylinder, C_{dovrms} is reduced with increasing Re expect for the case of test case within open terrain with lowest wind speed, (4) Regarding the effect of the terrain exposures, C_{dovrms} is higher for the case of suburban exposure due to the higher turbulence intensity.

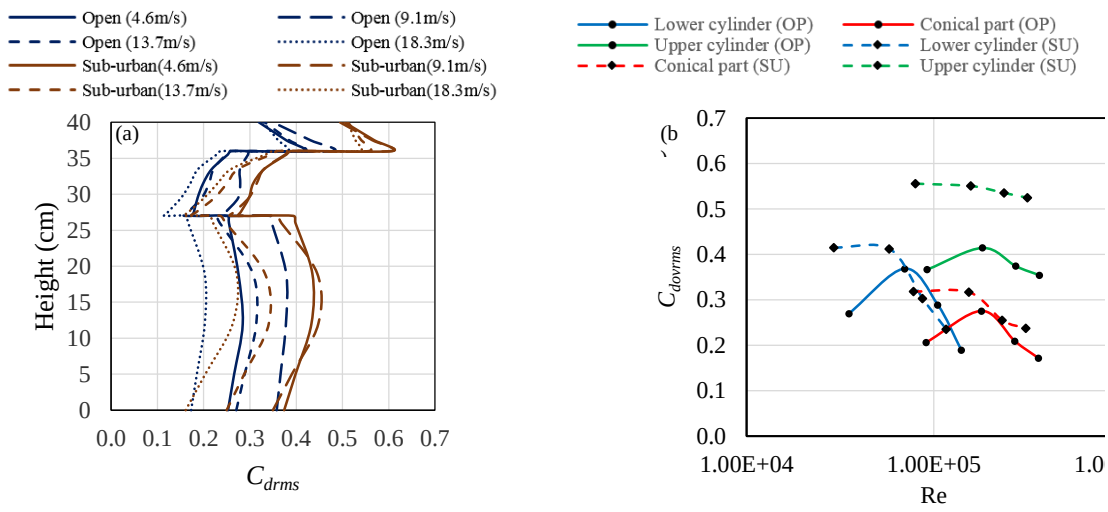

Figure 10: (a) Height-wise distribution of rms drag coefficient C_{drms}, (b) Variation of rms overall drag coefficient C_{dovrms} for each part with Re

5. CONCLUSIONS

In this study, a wind tunnel testing on scaled elevated conical tank models is performed in order to estimate the external wind pressures in addition to the total wind forces. The model is tested within a boundary layer using two terrain exposures which are open and suburban in order to assess the effect of the terrain exposure on the wind pressure values. In addition, each wind tunnel test corresponding to a terrain exposure is repeated for different wind speeds in order to assess the effect of changing Reynolds number on the measured pressures and the calculated forces.

The wind pressures' time series are recorded and both mean pressure coefficient C_{pm} and rms pressure coefficient C_{prms} are obtained over the model's surface for different test cases. By integrating the pressure coefficient, the mean drag coefficient C_{dm} is obtained at different heights and the following is concluded: (1) C_{dm} for the lower cylinder has a maximum value around the mid-height, while increasing linearly with the height for the conical part except for the lowest wind speed, and reduced with the height for the upper cylinder; (2) C_{dm} values for the suburban exposure are lower compared to the open-terrain. Integrating the mean drag C_{dm} over the height of each part will result in the overall drag coefficient C_{dovm} corresponding to each model part and it is concluded that C_{dovm} is higher for the case of open exposure due to the higher wind speed profile compared to the suburban one.

By plotting C_{dovm} for each part against Re, the following is concluded: (1) For the lower cylinder, C_{dovm} is reduced with increasing Re for different testing levels expect for the case of open terrain with lowest wind speed; (2) For the conical part, C_{dovm} is reduced by increasing Re for the cases where the lower cylinder is included expect for the case open terrain with lowest wind speed; (3) For the upper cylinder, C_{dovm} is slightly reduced for higher Re values

Following the same integration procedure for rms pressure coefficient, rms drag coefficient C_{drms} at different levels is obtained in addition to rms overall drag C_{dovrms} and the following is concluded: (1) C_{drms} distribution for the lower cylinder has a maximum value around the mid-height; (2) C_{drms} increases with the height for the conical part; (3) C_{drms} is reduced with the height for the top cylinder; (4) C_{drms} values for the suburban exposure are higher compared to the open terrain due to higher turbulence intensity. Regarding the overall drag coefficient, the following is concluded: (1) For the upper cylinder, C_{dovrms} is reduced with increasing Re expect for the case of within open terrain with lowest wind speed, (4) C_{dovrms} is higher for the case of suburban exposure due to the higher turbulence intensity.

By plotting C_{dovrms} for each part against Re, the following is concluded: (1) For the conical part, C_{dovrms} is reduced with increasing Re; (2) For the upper cylinder, C_{dovrms} is reduced with increasing Re expect for the test case within open terrain corresponding to lowest wind speed.

REFERENCES

ASCE, 2012. Wind Tunnel Testing for Buildings and Other Structures. Reston, VA: ASCE.

Baban, F. and So, R., 1991. Aspect ratio effect on flow-induced forces on circular cylinders in a cross-flow. Experiments in Fluids, 10:313-21.

BLWTL, 2007. Wind Tunnel Testing: A general outline. Western University, Boundary Layer Wind Tunnel.

ESDU, 1980. Mean forces, pressures and flow field velocities for circular cylindrical structures: single cylinder with two-dimensional flow. Engineering Sciences Data Unit , ESDU data item 80025.

Falcinelli, O.A. et al., 2011. Influence of Topography on Wind Pressures in Tanks Using CFD. Latin American Applied Research, 41:379-88.

Flores, F.G. and Godoy, L.A., 1998. Buckling of short tanks due to hurricanes. Engineering Structures, 20(8):752:60.

Fox, T. and West, G., 1993a. Fluid-induced loading of cantilevered circular cylinder in a low-turbulence uniform flow. Part 1: mean loading with aspect ratios in the range 4 to 30. Journal of Fluids and Structures, 7:1-14.

Godoy, L.A., 2007. Performance of Storage Tanks in Oil Facilities Damaged by Hurricanes Katrina and Rita. J. Perform. Constr. Facil., 21(6):441-49.

Macdonald, P.A. et al., 1988. Wind Loads on Circular Storage Bins, Silos And Tanks: I. Point Pressure Measurements on Isolated Structures. Journal of Wind Engineering and Industrial Aerodynamics, 31:165-88.

Okamoto, T. and Sunabahiri, Y., 1992. Vortex shedding from a circular cylinder of finite length placed on a ground plane. Journal of Fluids Engineering, 114:512-21.

Parammasivam , K.M. and Tamura, Y., 2007. Aerodynamic Characteristics of a Conical Water Tank. In Proceedings of the Annual Meeting, Japan Society of Fluid Mechanics., 2007.

Rossana , J.C. and Godoy, L., 2010. Wind buckling ofmetal tanks during their construction. Thin-walled structures, 48(6):453-459.

Sabransky, I.J. and Melbourne, W.H., 1987. Design Pressure Distribution on Circular Silos With Conical Roofs. Journal of Wind Engineering and Industrial Aerodynamics, 26:65-84.

Sundaravadivel, T.A. et al., 2009. CFD Prediction of Wind Pressures on Conical Tank. Journal of Wind Engineering, 65:45-55.

Uematsu, Y. et al., 2014. Design wind force coefficients for open-topped oil storage tanks focusing on the wind-induced buckling. Journal of Wind Engineering and Industrial Aerodynamics, 130:16-29.

Uematsu, Y. et al., 2015. Design wind loads for open-topped storage tanks in various arrangements. Journal of Wind Engineering and Industrial Aerodynamics, 138:77-86.